Nanoscale Bioreceptor Layers Comprising Carboxylated Polythiophene for Organic Electrochemical Transistor-Based Biosensors

Yunjia Song[†], Zachary D. Lamberty [†], Junhao Liang[†], Miguel Aller Pellitero[‡], Justine S. Wagner[†], Eugenie Jumai'an[†], Michael A. Bevan[†], Joelle Frechette[†], Netzahualcóyotl Arroyo-Currás[‡,†], and Howard E. Katz[†,*]

[†]Department of Materials Science and Engineering and Department of Chemical and Biomolecular Engineering, and Department of Biomedical Engineering, Johns Hopkins University, 3400 North Charles Street, Baltimore, MD, USA.

[‡]Department of Pharmacology and Molecular Sciences, Johns Hopkins University School of Medicine, 725 N. Wolfe St., Baltimore, MD, USA.

*corresponding author: email hekatz@jhu.edu

Abstract

We investigated the carboxylated conjugated polymer poly 3-(3-carboxypropyl) thiophene-2,5-diyl (PT-COOH) as a nanosized (200-350 nm) biomolecule receptor layer on the channel of organic electrochemical transistor (OECT) devices. Myelin Basic Protein (MBP), SARS-CoV-2 spike glycoprotein S1, and their antibodies (10-nm size scale) were alternately used in attached molecule form as receptors and analytes. Sub-ng detection in buffer was observed, and response to S1 was also obtained in clinical serum. Changes in threshold voltage (Vth) and current output from OECT transfer curves, and measurements of open circuit potential between receptor layers and a reference electrode provided complementary responses and insight into the response mechanisms, guiding further development of electrochemical field-effect and voltammetric protein sensors based on polymeric active layers with nanoscale functionality.

Keywords

Conjugated polymers, biosensors, myelin basic protein, SARS-CoV-2, OECT, open circuit potential, zeta potential

1. Introduction

Electronic biosensors based on conjugated polymers have been developed in recent decades because of the ease of attaching receptor functional groups and modulating electronic properties. [1-3] Multiple types of biomolecules can be detected through organic field-effect transistor (OFET)-based biosensors, including large and small molecules such as proteins (10-nm size scale), DNA, or ascorbic acid.[4-9] However, the need to detect lower concentrations of biomolecules and further sensing signal amplification is ever present. Device configurations including organic electrochemical transistors (OECT) have recently been developed to help meet this need.[10] OECTs are also three-terminal devices, but the gate voltage is applied through an electrolyte interfacing with an organic semiconductor.[11-12] Different types of materials are used in OFET and OECT based biosensors, each having its own advantages.[13-16] In a recent work from our group, Huang and co-workers reported that polystyrene-block-poly(acrylic acid) can be used in antibody immobilization on top of OFETs leading to responses to nmol/mL of negatively charged glial fibrillar acidic protein (GFAP), selectively over negatively charged bovine serum albumin (BSA).[17] Song and co-workers further showed that different types of antibody-functionalized copolymers on OFETs, with different arrangements and dilutions of carboxyl groups, responded to 10 ng/mL of positively charged myelin basic protein (MBP).[18] None of these polymers allowed hole or electron transport, though proton conduction may have been allowed.

Building from such prior work, we now use poly 3-(3-carboxypropyl) thiophene-2,5-diyl (PT-COOH), a conjugated hole-transporting polymer containing carboxylic acid groups on the side chains, for the first time as the receptor layer in an OECT detection configuration. This polymer had previously been reported as an OECT semiconductor, and our own group had used it in chemoresistive vapor sensors. [19,20] The structure of the polymer is shown in Scheme 1. We chose PT-COOH because its combination of a responsive and reactive functional group with π conjugation that allows for charge equilibration (mostly deprotonated/negatively charged carboxyl groups combined with

hole transport) has appeared promising for bioreceptor functionality. This is because receptors can be easily attached and electronic signatures of bioanalytes would be prominent. Based on previous work by our group,[21] PT-COOH presents a linear surface electrochemical response to pH in the range pH = 3-9, encompassing physiological pH. [19,21] This feature facilitates translation of the polymer receptor to allow biomolecular detection under physiological conditions (e.g., human serum).

The carboxylated thiophene is more compatible with aqueous physiological solutions than are the much less polar polymer OFET top gate dielectric materials and has a more direct coupling mechanism between the analyte solution and the source-drain current path. The result is a lower-concentration limit of detection. The high capacitance through the aqueous solution between the reference electrode and channel region makes it possible to measure the drain current change at a lower gate- drain voltage (for OFETs this may be about -50V, but for OECT devices as little as -1V). Furthermore, the COOH group allows for peptide coupling reactions to help ensure covalent linkage between receptor functional groups and the active electronic polymer film.

Our goal is to fabricate OECT-based immuno-biosensors capable of detecting immunoglobulins (antibodies) or their targets (antigens) (10-nm size scale) with high sensitivity (≤pg/mL). The OECT configuration is ideal for this application because it can capture both interfacial potential and impedance changes that result from antibody-target binding. In addition, we seek to understand the target properties that generate significant OECT responses to support rational design of future biosensors. As model systems, we focus on the detection of myelin basic protein (MBP) and SARS-CoV-2 Spike 1 protein antibody. MBP is critical to central nervous system myelin homeostasis and has various functions; too low a concentration of MBP can lead to diseases like demyelinating autoimmune disease, so monitoring its concentration can be essential. [22-23] MBP has a decidedly net positive charge at physiological pH, and the interaction between MBP and MBP antibody can be detected through electrochemical

measurements. [24] Thus, we chose MBP and MBP antibody as antibody and antigen pair to optimize our testing configuration as well as the biomolecule interaction condition. Based on the results obtained in the MBP experiment, we extended the investigation to a second antigen-antibody pair interaction as described below.

Since 2019, the global pandemic caused by the SARS-CoV-2 virus is still an unsolved problem. Fast and low-cost detection methods of the virus particles or antibodies are needed as tools for monitoring and stopping the pandemic. Many biosensing devices based on different mechanisms have been developed to help the diagnosis of the disease. [25-29] The reverse transcription polymerase chain reaction (RT-PCR) can be used as a preliminary method to detect the SARS-CoV-2 virus. Chu and coworkers use sputum samples from patients in RT-PCR assays to specifically detect the viral RNA.[29-30] Giwan Seo and coworkers developed an FET-based biosensor to detect the SARS-CoV-2 virus, where antibodies were immobilized on a graphene surface, and the electrical signals were monitored with the change of concentration of the antigens.[25] Qiu and coworkers designed a biosensor based on localized surface plasmon resonance (LSPR), which can detect binding events. The sensing chips were functionalized with the thiol-cDNA receptor and, after injection of RNA-dependent RNA polymerase (RdRp) from COVID-19 samples, a sensing signal can be revealed through localized surface plasmon resonance (LSPR).[27,31] Guo and coworkers just published a paper based on OECT devices related to SARS-CoV-2 detection. They chose poly(ethylenedioxythiophene) polystyrenesulfonate (PEDOT:PSS) and the alkoxylated thiophene polymer p(g0T2-g6T2) as the channel material and functionalized the gold electrode with nanobodies to detect the target.[32] Although these works were pioneering, efforts are still critically needed to further expand the arsenal of diagnostics that can be used to address the current pandemic, or rapidly adapted to functionally respond to future ones.

We show here that PT-COOH can be covalently linked to the MBP antibody through N-ethyl-N′-(3-dimethylaminopropyl)carbodiimide/N-hydroxysuccinimide (EDC/NHS)

coupling chemistry, and the interaction between MBP and anti-MBP antibody on PT-COOH can be detected through our OECT configuration. We further discovered that PT-COOH can also be a good medium for observing the interaction between the receptor-binding domain (RBD) of SARS-CoV-2 virus and S1 protein antibody. As an alternative to enzyme-linked immunosorbent assays (ELISAs), which are the benchmark detection strategy for antibody-antigen interactions in the clinic, our method using the OECT active device is a label-free method and can quickly detect affinity interactions.[33-35] Also, because the polymer we chose has carboxylic acid groups in the side chains, immobilization of antibodies or proteins is simple and achievable at high yield via carbodiimide coupling. Since our OECTs can detect the interaction between RBD and S1 protein antibody and can differentiate positive and negative clinical samples, the proposed platform has potential use in SARS-CoV-2 virus detection and antibody concentration monitoring. In addition, we demonstrate that open circuit potential (OCP) measurements can be performed on films deposited on the same substrates as those used for OECT devices and directly measure the potential change between the working and the reference electrodes in the devices. The responses from OECT transfer curves and OCP measurements were specific and self-consistent. Covalent attachment of antibody to PT-COOH also induced a large zeta potential change. This broadens the evidence that protein attachment to PT-COOH is possible and that the functionalized PT-COOH functions effectively as a receptor layer.

2. Experimental section

2.1 Main Reagents

N,N-Dimethylformamide (DMF), 99.8%, Extra Dry, was purchased from Fisher Scientific and was produced by ACROS Organics in Belgium, catalog number AC326871000. Poly [3-(3-carboxypropyl)thiophene-2,5-diyl] regioregular (PT-COOH) was purchased from Rieke metals in Nebraska; its catalog number is 4030. PBS solution was bought from Thermo Fisher Scientific; its catalog number is 10010023. Anti-Myelin Basic Protein (MBP) antibody and Myelin Basic Protein (MBP) were both bought from Sigma Aldrich in Burlington; anti-MBP has a catalog number M3821 and

MBP has a catalog number M0689. N-(3-Dimethylaminopropyl)-N′-ethylcarbodiimide hydrochloride (EDC) and N-Hydroxysulfosuccinimide sodium salt were also bought from Sigma Aldrich; the catalog number of EDC is E6383 and of NHS is 56485. Albumin, Bovine, Fraction V, 97% (BSA) was obtained from Alfa Aesar in Massachusetts; its catalog number is J64655. Glutaraldehyde solution , 50% (GA hydrogel) was bought from Fisher Scientific, its catalog number is G151-1. (3-Aminopropyl)triethoxysilane (APTES) was bought from Sigma Aldrich; its catalog number is 440140. Sulfate Latex Beads, 8% w/v, 0.1 μm (Sulfate functionalized polystyrene latex particles) was bought from Thermo Fisher Scientific; its catalog number is S37204. Interdigitated Electrode Arrays for Biochemical Sensors were obtained from NanoSPR in Chicago, with 10mkm gap and 20mkm finger.

2.2 Conjugated polymer film formation for OECTs

OECT interdigitated electrodes obtained from NanoSPR were cleaned by immersion in isopropanol for 15 min. Then, the substrates were treated with UV-ozone for 30 min. PT-COOH was dissolved in dimethylformamide (DMF) and heated at 130 °C for 10-15 min to a final concentration of 20 mg/mL. The solution was filtered through a 0.45um PTFE filter after cooling. PT-COOH solution was applied to the OECT devices on glass substrates and spin-coated for 320 s at 1600 rpm. The films were kept in a glovebox at 70 °C overnight to remove the solvent. The film thickness was in the range of 200-350 nm, measured using a Filmetrics F20-NIR thin film analyzer.

For making polymer films for the surface zeta potential measurement, the PT-COOH solution was deposited on clean glass slides functionalized with the adhesion promoter (3-aminopropyl)triethoxysilane (APTES) to enhance the stability of the PT-COOH film. The glass slides were cleaned with piranha solution (3:1 H_2SO_4:H_2O_2) for at least 1 hour, followed by O_2 plasma treatment (50 W, 2 min, ≈300 mTorr). To functionalize the glass slides with APTES, we immersed them in unagitated solutions of 50 mL toluene:1 ml APTES for 1 h, followed by rinsing (toluene, ethanol, and water), and annealing at 100^{o}C for 15 min. PT-COOH films were prepared by dissolving a solution of 20 mg/mL

PT-COOH in DMF and spin-coating the solution onto the APTES-functionalized glass slides at 3000 rpm followed by annealing overnight to remove excess solvent.

2.3 Antibody immobilization

The antibodies were immobilized using a surface immobilization method. The first step was to activate the carboxylic acid groups in the already-formed PT-COOH films. EDC/NHS was dissolved in distilled water with a concentration of 10 mg/ml and 3 mg/ml, respectively. The EDC/NHS solution was added onto the top of a PT-COOH film and left for 20 min. The polymer film was then rinsed with 0.05X or 1X phosphate buffer solution (1X PBS: 144 mg/ml KH_2PO_4, 58 mg/ml NaCl, and 268 mg/ml Na_2HPO_4-7 H_2O, pH = 7.4) several times (different PBS concentration for different experiments). 100 μg/ml antibody was placed on the activated polymer film surface and left for 4 hours after the activation step. 100 μg/ml antibody solution was derived from the dilution of the original antibody solution by 1X PBS.

Before performing any electrical measurements, 0.05 ml bovine serum albumin (BSA) at a concentration of 10 mg/ml was placed on the antibody-immobilized PT-COOH film for 30 min to form a blocking layer to prevent nonspecific binding. Scheme 1 shows the schematic images of the immobilization geometry.

2.4 Protein immobilization

OECT devices (covered with PT-COOH films) were immersed in a mixture of BSA solution and glutaraldehyde (1:1 volume ratio) overnight to enhance the immobilization of BSA on the polymer films. After mixing, the final concentration of BSA solution is 5mg/ml and the concentration of glutaraldehyde is 1%(w/w) Then the OECT devices were immersed in 1X PBS solution for 10 min to remove the unattached BSA. After that, the carboxylic groups on BSA were activated by EDC/NHS chemistry and linked to MBP or SARS CoV-2 RBD. The protein was left on the top of BSA for an hour at room temperature to finish the attachment. The immobilization geometry is shown in Scheme 2.

2.5 Transfer curve sensing measurement on OECTs

The channel region of the OECT devices, which was covered with biomolecule-functionalized polymer films, was connected to the gate probe through an Ag/AgCl reference electrode with electrolyte in between. Before the start of electrical sensing signal measurement, the functionalized channel region was covered with PBS solution and transfer curves were repeatedly measured until they overlapped each other for stabilization. After this stabilization process, different concentrations of analyte were added between the reference electrode and the channel region of OECT interdigitated electrodes, and then the transfer curves were measured, obtaining the threshold voltages and current differences.

2.6 Surface zeta potential measurement

Surface zeta potential measurements [36] were performed using a Malvern Zetasizer NanoZS with the SZP accessory ZEN1020. The coated glass slices were attached to the sample holder using 3M VHB tape. Sulfate-functionalized polystyrene latex particles (SLPs) of 100 nm diameter act as probes for the zeta potential. The SLPs were dispersed at a ratio of 1 μL/ 8 mL in a solution of PBS buffer diluted to have a conductivity of ≈ 500 μS/cm and pH ≈ 7.4. The accessory is immersed in the solutions containing the tracer particles for measurements. The SLPs have a stable negative zeta potential of around −50 mV at pH 7.4. We follow the protocol in Karnal et al. based on the work of Corbett et al. to obtain the zeta potential of the coated surface. Each measurement is repeated on at least 7 samples from at least 3 batches, and the average value is reported along with the standard deviation. [37,38]

2.7 OCP measurement

Open circuit potential (OCP) measures the potential difference between the reference and working electrode without applying any voltages. [10,11] The schematic image of our OCP measurement configuration is shown in Scheme 3. In our setup, Ag/AgCl acts as the reference electrode, and the working electrode is the same combination of electrodes

and active film as for the OECT device. The drain was connected to the potentiostat. In this case, the OCP measurement can detect the potential difference caused by the channel region functionalization.

2.8 Clinical Specimens

Access to the clinical specimens employed in this work was granted by the Johns Hopkins COVID-19 Clinical Research Coordinating Committee, under approved IRB protocol # IRB00250000. All specimens were obtained with consent by trained medical personnel, stripped from any HIPPA-defined identifying information, and stored in a safe COVID-19 specimen repository. The specimens employed in this work were immediately destroyed after use in compliance with safety and regulatory protocols.

3. Results and discussion

3.1 OECT transfer curve measurement

3.1.1. MBP antibody immobilized on PT-COOH & MBP as analyte in 0.05 X PBS.

The initial Vth of PT-COOH in an OECT with PBS electrolyte is -0.32 V with a standard deviation of 0.05. The interaction between MBP and its antibody changed the threshold voltages of the devices. Figure S1(a) shows the transfer curves of the MBP-MBP antibody pair main experiment and Figure S1 (b) shows the control experiment without anti-MBP antibody immobilization, but with BSA blocking layer and the application of MBP as analyte in 0.05 X PBS. To specify the sensing signals with a numerical parameter, the changes of the threshold voltages were calculated. In Figure 1, the black curve represents the threshold voltages calculated from main experiments and the red curve represents the threshold voltages calculated from control experiments. ΔVth represents the threshold voltage change after adding MBP solutions compared to using only PBS in the place of analyte between the reference electrode and the channel region. The range of threshold voltage change is different between main and control experiments. For the main experiment, the threshold voltages decrease with increasing concentrations of MBP, and the difference can reach -0.08V with a standard deviation of 0.009, which means the threshold voltages become more negative after adding

MBP—the OECTs become more difficult to turn on. As for the control experiment, the average change of threshold voltage fluctuates between 0.00 V -0.02V. The change in threshold voltages is also illustrated in Figure 1 . The interaction between MBP and anti-MBP changing the surface potential of the channel region can lead to the decrease of the threshold voltage. The MBP protein has a positive charge at physiological pH.[39] Thus, when MBP was added to the antibody- functionalized surface, the surface charges at the interfaces of the PT-COOH films become more positive, and the accumulation of the positive charge will repel positive charge carriers away from the channel region (or increase the negative gate voltage required to induce and compensate for mobile positive charges in the OECT, which decreases the source-drain hole current in the p-type polymer, thereby making the threshold voltages become more negative with the increasing concentration of MBP).

3.1.2 MBP antibody immobilized on PT-COOH & MBP as analyte in 1X PBS.

To determine the extent to which voltage changes might depend on using diluted PBS, we did the same MBP-MBP antibody interaction experiment in 1X PBS. The average threshold voltages and the change in threshold voltages are shown in Figure 2. The figures are the average threshold voltage and threshold voltage change after we added MBP as analyte. It can be observed that the change in threshold voltages becomes smaller, but there is still a -0.04V change despite the additional screening by the more concentrated buffer ions. The increasing concentration of buffer solution does decrease the sensitivity to some extent, because the additional ions in the PBS solution can penetrate inside the channel region and cause electric field screening, but the interaction between antibody and antigen can still be detected.

3.1.3 MBP immobilized on PT-COOH & anti-MBP as analyte.

Besides antibody immobilization on PT-COOH, we also immobilized MBP on PT-COOH films. For this sensing configuration, MBP antibodies were the analyte. Figure 3 indicates the average threshold voltages for different experiments. The MBP+MBP

antibody experiment is the main experiment, and the BSA+ MBP antibody is one of the control experiments where only BSA was immobilized in the polymer and no MBP was linked to it. The MBP+cortisol antibody is another control experiment to determine the specificity of the experiment. Based on the results, it can be deduced that the threshold voltage change is only caused by the specific binding of MBP antibody to the polymer surface-immobilized MBP. The maximum scale of the threshold voltage change is about -0.025V, with a standard deviation of 0.009V, which is smaller than the voltage change in the antibody-immobilized experiment, but in the opposite direction. That effect may be because the MBP antibody does not carry as much charge as MBP, so the scale of threshold voltage change is not equivalent. In addition, it can also be because the interaction between MBP and MBP antibody neutralizes some of the positive charges carried by MBP, decreasing their effect so the p-type OECTs become easier to turn on. This would be consistent with the positive charges brought by MBP decreasing the effective negative voltage imposed by the gate, so that the increase in negative gate voltage needed for turn on because of the MBP present is not as great when the antibody binds to it. There are multiple examples of electrostatic effects from receptor-biomolecule binding to organic electronic devices, and the relationship between biomolecule charge and threshold voltage shift can vary depending on the electrostatics of each system. [4, 17,18].

3.1.4 RBD immobilized on PT-COOH & SARS-CoV-2 Spike 1 (S1) protein antibody as analyte.

Based on results obtained in the MBP experiments, we explored the utility of analogous experiments for SARS-CoV-2-related biomolecule detection. We tried the S1 antibody immobilization method to see if we could detect the RBD of the virus, and the RBD protein immobilization method to see if we could detect the anti-S1 protein antibody. The protein immobilization method shows better results, as shown in Figure 4. Covalent linkage of BSA to PT-COOH gave a more negative Vth of -0.37 V, in contrast to the physisorption of BSA described above. This shift was partially compensated with the further attachment of RBD, while attachment of anti-S1 had little further effect. The

main experiment, with largest signal, is the RBD+ S1 antibody pair. Figure 4 illustrates that only the main experiment (RBD with the corresponding S1 antibody) shows a threshold voltage change (significant downward slope, shown by the black curve). The threshold voltages of the control experiments both fluctuate in a 0.01V range. The maximum threshold voltage change of the main experiment is around -0.04V. We also analyzed current changes induced by anti-S1 binding. First, the gate leakage current was subtracted from all the drain currents, and then the ratio of the resulting currents with and without analyte was calculated. The numerators were the currents obtained when the different concentrations of antibody were added, and the denominator was the current obtained when no antibody was added (only PBS). We found that the current change is a more proper indication of sensing signal. In Figure 4, the current continuously decreases when the concentration increases, and the ratio of the currents at high and zero concentrations ultimately reaches 54%, obviously different from the control experiments. T-tests were also done to determine whether the results of the main experiment based on current changes were significantly different from each of the two control experiments, one with linked BSA but no RBD, and the other with anti-MBP (mismatched) as the analyte instead of S1 antibody. Results are shown in Table S1. Figure 4 and Table S1 illustrate that the limit of detection (LOD) of this antibody detection configuration is 10fg/ml. The null hypothesis is that the data of the main experiment are the same as the control experiments. At 10fg/ml, the absolute values of t stat are larger than the values of t critical, and the p values are all smaller than 0.05, demonstrating that there is more than 95% possibility that our null hypothesis is not correct, so our main experiment is significantly different from the control experiments.

We also observed that with increasing anti-S1 antibody concentrations, the current decreases and the absolute value of threshold voltages increases. Furthermore, RBD should be positively charged, [40,41] though it is linked via negatively charged BSA. The linking of BSA to the PT-COOH seems to trap holes, making Vth more negative, while subsequent binding of RBD has the reverse effect, and anti-S1 seems to rearrange the

positive and negative charges from the bound RBD and BSA so that they again trap mobile holes in the PT-COOH, meaning that the response is not simply electrostatic [4,17,18]. Recalling the total film thickness of 200-350 nm, this entire charge rearrangement is obviously on the nanoscale.

3.2 Zeta potential measurement.

The surface Zeta potential results are indicated in Figure 5. The Zeta potential of PTCOOH film was found to be -77 ± 2 mV. The negative value of the zeta potential is consistent with the presence of carboxylic acid groups. The hydrogen atom can transfer from the carboxylic acid groups to bases dissolved in the water and leave predominantly negatively charged deprotonated carboxyl groups on the surface. The fact that these groups are electronically influential supports the idea that antibodies coupled to them via the EDC-NHS activation mechanism will be capable of signaling antigen binding events. After the immobilization of the antibody, the negative value decreases, which can be a proof that some of the carboxylic acid groups successfully bind to the MBP antibody; the negative charge created by the carboxylic acid groups are neutralized by the immobilized antibodies. After adding BSA, the zeta potential does not change significantly., The reason may be that although BSA can cover the unreacted carboxylic acid groups, BSA itself carries a negative charge at pH 7.4[42], so the overall surface zeta potential change is not that obvious. After the binding of MBP, the surface zeta potential change is again not significant compared to the uncertainty of the measurement. Despite the positive charge of the MBP, [39,43], the dipolar orientation of the MBP, antibody, and counterions could result in a compensating negative potential at the interface. Also, because the 100-nm tracer particle used contains anionic sulfate groups on the surface, they could be sufficiently attracted to the MBP coatings to simply bind to them and thereby neutralize some of the positive charges brought by the MBP. Comparing the results we obtained from the zeta potential measurement and the results from the OECT measurements, it can be observed that OECT shows a stronger voltage response to antibody-antigen interaction. These differences possibly result from the

geometry of the two measurements. There is an applied potential in the zeta potential experiment in the horizontal direction of the samples while potentials in the near-interface liquid layer are sensed. On the other hand, voltage is applied in the OECT devices from the top gate to the bottom source/drain, so a greater thickness of electroactive film can be affected.

3.3 OCP measurement

3.3.1 OCP measurement on MBP antibody & MBP samples.

The OCP measurement was done on pure PT-COOH films, MBP antibody-immobilized PT-COOH films and MBP-added films. The potential of pure PT-COOH films is 40 ± 2mV. After antibody immobilization, the OCP decreases slightly to 35 ± 6mV, which indicates that the antibodies do not have obvious net charges, or are influenced by the negatively charged BSA that is also applied. Physisorption of BSA induced a significant negative shift to 12 ± 3mV. After adding the MBP, the OCP has an obvious increase, which increases from 12 ±3mV to 30 ± 3mV, as shown in Figure 6(a). This is consistent with the MBP-induced threshold voltage changes. By contrast, attachment of MBP as the receptor increased OCP to 52 ± 10mV, and interaction with anti-MBP as analyte brought the potential to more negative values (Figure S2).

3.3.2 Open circuit potential measurement on RBD & S1 antibody samples.

Before detecting the RBD and S1 antibody interaction, BSA-only embedded samples and RBD-immobilized samples were tested by OCP measurement, and the results are listed in Table S2. When BSA with negative charges was immobilized on the polymer film, the potential becomes more negative and goes from 40 mV to 22 mV. After the linkage of RBD, since the RBD is positively charged, the OCP becomes larger and reaches 53 mV. After adding the S1 protein antibody, some of the positive charges of RBD were neutralized by the S1 protein antibody, so the potential decreases while the concentration of the S1 antibody increases (Figure 6(b)). Finally, the antibody appeared to saturate the RBD at 10 ng/ml.

3.3.3 OCP measurement on RBD & clinical samples.

After doing the open circuit measurement on the commercial RBD and S1 protein antibody pair, we tested the interaction between RBD immobilized samples and clinical samples. The clinical samples were sequentially diluted down to concentrations 1:10, 1:100, 1:1000 and 1:10000, and were measured from low concentration to high concentration. Both positive and negative samples are measured, and it can be deduced that the seronegative clinical samples are more negatively charged, while seropositive samples are less negatively charged. However, the most obvious signals seem to come from the undiluted samples. To determine the LOD of the clinical samples, another set of same measurements but with small dilution ratio were measured, and the results are shown in Figure 7 and Figure S3. From a dilution ratio of 1/8, a difference in the OCP can be detected, and the undiluted samples still have the largest difference of surface potential. The commercially available S1 protein antibody was added to the same set of seropositive samples to prove the OCP trend change is similar with the commercial RBD and the clinical samples, which is further evidence of the interaction between the protein and the antibody. 10 μg/ml S1 protein antibody was added into 10 μl serum from the positive samples. From Figure 7, it can be observed that the OCP was decreased after adding the S1 protein antibody, and the change of the OCP is also more negative after adding the antibody. The decrease of OCP matches with the tendency that we previously observed with the RBD and S1 protein antibody pair. After adding the S1 protein antibody in the clinical samples, the antibody can interact with the virus protein in the clinical samples as well as the RBD, which can cause the decrease of the OCP. To draw a conclusion from the clinical samples experiment, the average OCP of the negative samples is more negative than the positive samples, which can be used to differentiate seropositive and seronegative cases.

4.Conclusion

A summary of all the OECT and OCP results is presented in Table 1. The methods provide complementary and independent means of interrogating the interfacial potential changes as a result of surface binding events, all of which occurred in films on the hundreds of nm size scale in thickness, or in interfacial regions extending a few nm from the film surfaces. The OCP measurement is a direct measurement of the surface potential relative to a reference electrode while the OECT measurement includes a lateral source-drain voltage and reports the combined changes in the charge distribution and mobility in the responsive film. Both can inform about the interactions between antibodies and antigens, and in combination can help evaluate the importance of surface potential and other electronic effects to the interactions. The absolute measured currents for OECTs are higher relative to instrument limits compared to OCP voltages, and the best OECT signals are a factor of 2-4 higher than the experimental uncertainties. On the other hand, the best OCP signals were about 5x higher than the uncertainties. All of the experiments involving MBP are electronically self-consistent. Attachment of a net-negative charge protein (or covering a positive protein) and the converse arrangements (attachment of a net-positive charge protein or covering a negative protein) shift Vth more positive, or in the converse case, more negative, respectively. The OCP changes in response to these actions are exactly the opposite, since they measure voltage at the polymer surface rather than the gate reference electrode and indicate the net charge of the last protein attached or adsorbed. For the anti-S1 experiments, the OCP changes were one again consistent with the net charge of the last protein attached or adsorbed. However, as pointed out above, the Vth changes were not the opposite of the OCP changes, indicating a mechanism involving charge distributions further into the bulk of the polymer.

We developed our recently proposed idea that the conjugated polymer PT-COOH can act as a bioreceptor layer with covalent attachment of an antibody or immobilize protein.

We use the label-free OECT measurement, open circuit potential measurement and surface zeta potential measurement to show that antibody and protein embedded immobilization method can be achieved. The threshold voltage or current changes in the OECT measurement caused by the interaction between MBP and anti-MBP antibody or RBD and S1 protein antibody on PT-COOH films can be a useful signal for designing an immuno-biosensor. An amplification of signals or higher reproducibility can be investigated for future research.

Supporting information. The Supporting Information is available free of charge at … Additional transfer curves, OCP data, and statistical data.

Acknowledgements

Research reported in this publication was supported by the National Science Foundation (NSF) Division of Materials Research, Grant number 1807292. We are grateful to Dr. Hyun-June Jang for initial configuration of the OECT. M.A.P. and N.A-C thank the JHU COVID-19 Research Response Program and COVID-19 Clinical Research Coordinating Committee for financial support and access to clinical specimens from established biorepositories.

Conflict of interest

The authors declare no conflict of interest.

References

1. Kergoat, L.; Piro, B.; Berggren, M.; Horowitz, G.; Pham, M.-C. Advances in Organic Transistor-Based Biosensors: From Organic Electrochemical Transistors to Electrolyte-Gated Organic Field-Effect Transistors. Anal Bioanal Chem 2012, 402 (5), 1813–1826. https://doi.org/10.1007/s00216-011-5363-y.
2. Dailey, J.; Li, H.; Song, J.; Besar, K.; Jang, H.-J.; Chu, Y.; Katz, H. E. Material and Circuit Design for Organic Electronic Vapor Sensors and Biosensors. In Organic and Hybrid Sensors and Bioelectronics XII; SPIE, 2019; Vol. 11096, pp 14–21. https://doi.org/10.1117/12.2530058.
3. Li, H.; Shi, W.; Song, J.; Jang, H.-J.; Dailey, J.; Yu, J.; Katz, H. E. Chemical and Biomolecule Sensing with Organic Field-Effect Transistors. Chem Rev 2019, 119 (1), 3–35. https://doi.org/10.1021/acs.chemrev.8b00016..
4. Khan, H. U.; Roberts, M. E.; Johnson, O.; Förch, R.; Knoll, W.; Bao, Z. In Situ, Label-Free DNA Detection Using Organic Transistor Sensors. Advanced Materials 2010, 22 (40), 4452–4456. https://doi.org/10.1002/adma.201000790.
5. Hammock, M. L.; Knopfmacher, O.; Naab, B. D.; Tok, J. B.-H.; Bao, Z. Investigation of Protein Detection Parameters Using Nanofunctionalized Organic Field-Effect Transistors. ACS Nano 2013, 7 (5), 3970–3980. https://doi.org/10.1021/nn305903q.
6. Minamiki, T.; Sasaki, Y.; Tokito, S.; Minami, T. Label-Free Direct Electrical Detection of a Histidine-Rich Protein with Sub-Femtomolar Sensitivity Using an Organic Field-Effect Transistor. ChemistryOpen 2017, 6 (4), 472–475. https://doi.org/10.1002/open.201700070.
7. Magliulo, M.; De Tullio, D.; Vikholm-Lundin, I.; Albers, W. M.; Munter, T.; Manoli, K.; Palazzo, G.; Torsi, L. Label-Free C-Reactive Protein Electronic Detection with an Electrolyte-Gated Organic Field-Effect Transistor-Based Immunosensor. Anal Bioanal Chem 2016, 408 (15), 3943–3952. https://doi.org/10.1007/s00216-016-9502-3.
8. Minamiki, T.; Minami, T.; Kurita, R.; Niwa, O.; Wakida, S.; Fukuda, K.; Kumaki,

D.; Tokito, S. A Label-Free Immunosensor for IgG Based on an Extended-Gate Type Organic Field Effect Transistor. Materials 2014, 7 (9), 6843–6852. https://doi.org/10.3390/ma7096843.

9. Gualandi, I.; Marzocchi, M.; Scavetta, E.; Calienni, M.; Bonfiglio, A.; Fraboni, B. A Simple All-PEDOT:PSS Electrochemical Transistor for Ascorbic Acid Sensing. J. Mater. Chem. B 2015, 3 (33), 6753–6762. https://doi.org/10.1039/C5TB00916B.
10. Strakosas, X.; Bongo, M.; Owens, R. M. The Organic Electrochemical Transistor for Biological Applications. Journal of Applied Polymer Science 2015, 132 (15), 41735. https://doi.org/10.1002/app.41735.
11. Moser, M.; Savagian, L. R.; Savva, A.; Matta, M.; Ponder, J. F.; Hidalgo, T. C.; Ohayon, D.; Hallani, R.; Reisjalali, M.; Troisi, A.; Wadsworth, A.; Reynolds, J. R.; Inal, S.; McCulloch, I. Ethylene Glycol-Based Side Chain Length Engineering in Polythiophenes and Its Impact on Organic Electrochemical Transistor Performance. Chem. Mater. 2020, 32 (15), 6618–6628. https://doi.org/10.1021/acs.chemmater.0c02041.
12. Bernards, D. A.; Malliaras, G. G. Steady-State and Transient Behavior of Organic Electrochemical Transistors. Advanced Functional Materials 2007, 17 (17), 3538–3544. https://doi.org/10.1002/adfm.200601239.
13. Heeger, P. S.; Heeger, A. J. Making Sense of Polymer-Based Biosensors. PNAS 1999, 96 (22), 12219–12221. https://doi.org/10.1073/pnas.96.22.12219.
14. Aydemir, N.; Malmström, J.; Travas-Sejdic, J. Conducting Polymer Based Electrochemical Biosensors. Phys. Chem. Chem. Phys. 2016, 18 (12), 8264–8277. https://doi.org/10.1039/C5CP06830D.
15. Liu, J.; Agarwal, M.; Varahramyan, K. Glucose Sensor Based on Organic Thin Film Transistor Using Glucose Oxidase and Conducting Polymer. Sensors and Actuators B: Chemical 2008, 135 (1), 195–199. https://doi.org/10.1016/j.snb.2008.08.009.
16. Gerard, M.; Chaubey, A.; Malhotra, B. D. Application of Conducting Polymers to Biosensors. Biosensors and Bioelectronics 2002, 17 (5), 345–359. https://doi.org/10.1016/S0956-5663(01)00312-8.

17. Huang, W.; Besar, K.; LeCover, R.; Dulloor, P.; Sinha, J.; Hardigree, J. F. M.; Pick, C.; Swavola, J.; Everett, A. D.; Frechette, J.; Bevan, M.; Katz, H. E. Label-Free Brain Injury Biomarker Detection Based on Highly Sensitive Large Area Organic Thin Film Transistor with Hybrid Coupling Layer. Chem. Sci. 2013, 5 (1), 416–426. https://doi.org/10.1039/C3SC52638K.
18. Song, J.; Dailey, J.; Li, H.; Jang, H.-J.; Russell, L.; Zhang, P.; Searson, P. C.; Wang, J. T.-H.; Everett, A. D.; Katz, H. E. Influence of Bioreceptor Layer Structure on Myelin Basic Protein Detection Using Organic Field Effect Transistor-Based Biosensors. Advanced Functional Materials 2018, 28 (37), 1802605. https://doi.org/10.1002/adfm.201802605.
19. Khau, B. V.; Savagian, L. R.; De Keersmaecker, M.; Gonzalez, M. A.; Reichmanis, E. Carboxylic Acid Functionalization Yields Solvent-Resistant Organic Electrochemical Transistors. ACS Materials Lett. 2019, 1 (6), 599–605. https://doi.org/10.1021/acsmaterialslett.9b00373.
20. Wagner, J.; Jang, H.-J.; Han, J.; Katz, H. E. Enhanced and Unconventional Responses in Chemiresistive Sensing Devices for Nitrogen Dioxide and Ammonia from Carboxylated Alkylthiophene Polymers. Mater. Horiz. 2020, 7 (5), 1358–1371. https://doi.org/10.1039/D0MH00049C.
21. Jang, H.-J.; Wagner, J.; Song, Y.; Lee, T.; Katz, H. E. Carboxylic Acid-Functionalized Conjugated Polymer Promoting Diminished Electronic Drift and Amplified Proton Sensitivity of Remote Gates Compared to Nonpolar Surfaces in Aqueous Media. Advanced Electronic Materials 2020, 6 (7), 1901073. https://doi.org/10.1002/aelm.201901073.
22. Boggs, J. M. Myelin Basic Protein: A Multifunctional Protein. Cell. Mol. Life Sci. 2006, 63 (17), 1945–1961. https://doi.org/10.1007/s00018-006-6094-7.
23. Träger, J.; Widder, K.; Kerth, A.; Harauz, G.; Hinderberger, D. Effect of Cholesterol and Myelin Basic Protein (MBP) Content on Lipid Monolayers Mimicking the Cytoplasmic Membrane of Myelin. Cells 2020, 9 (3), 529. https://doi.org/10.3390/cells9030529.

24. Tsekenis, G.; Garifallou, G.-Z.; Davis, F.; Millner, P. A.; Gibson, T. D.; Higson, S. P. J. Label-Less Immunosensor Assay for Myelin Basic Protein Based upon an Ac Impedance Protocol. Anal. Chem. 2008, 80 (6), 2058–2062. https://doi.org/10.1021/ac702070e.
25. Seo, G.; Lee, G.; Kim, M. J.; Baek, S.-H.; Choi, M.; Ku, K. B.; Lee, C.-S.; Jun, S.; Park, D.; Kim, H. G.; Kim, S.-J.; Lee, J.-O.; Kim, B. T.; Park, E. C.; Kim, S. I. Rapid Detection of COVID-19 Causative Virus (SARS-CoV-2) in Human Nasopharyngeal Swab Specimens Using Field-Effect Transistor-Based Biosensor. ACS Nano 2020, 14 (4), 5135–5142. https://doi.org/10.1021/acsnano.0c02823.
26. Bhalla, N.; Pan, Y.; Yang, Z.; Payam, A. F. Opportunities and Challenges for Biosensors and Nanoscale Analytical Tools for Pandemics: COVID-19. ACS Nano 2020, 14 (7), 7783–7807. https://doi.org/10.1021/acsnano.0c04421.
27. Asif, M.; Ajmal, M.; Ashraf, G.; Muhammad, N.; Aziz, A.; Iftikhar, T.; Wang, J.; Liu, H. The Role of Biosensors in Coronavirus Disease-2019 Outbreak. Current Opinion in Electrochemistry 2020, 23, 174–184. https://doi.org/10.1016/j.coelec.2020.08.011.
28. Srivastava, M.; Srivastava, N.; Mishra, P. K.; Malhotra, B. D. Prospects of Nanomaterials-Enabled Biosensors for COVID-19 Detection. Science of The Total Environment 2021, 754, 142363. https://doi.org/10.1016/j.scitotenv.2020.142363.
29. Santiago, I. Trends and Innovations in Biosensors for COVID-19 Mass Testing. ChemBioChem 2020, 21 (20), 2880–2889. https://doi.org/10.1002/cbic.202000250.
30. Chu, D. K. W.; Pan, Y.; Cheng, S. M. S.; Hui, K. P. Y.; Krishnan, P.; Liu, Y.; Ng, D. Y. M.; Wan, C. K. C.; Yang, P.; Wang, Q.; Peiris, M.; Poon, L. L. M. Molecular Diagnosis of a Novel Coronavirus (2019-NCoV) Causing an Outbreak of Pneumonia. Clinical Chemistry 2020, 66 (4), 549–555. https://doi.org/10.1093/clinchem/hvaa029.
31. Qiu, G.; Gai, Z.; Tao, Y.; Schmitt, J.; Kullak-Ublick, G. A.; Wang, J. Dual-

Functional Plasmonic Photothermal Biosensors for Highly Accurate Severe Acute Respiratory Syndrome Coronavirus 2 Detection. ACS Nano 2020, 14 (5), 5268–5277. https://doi.org/10.1021/acsnano.0c02439.

32. Guo, K.; Wustoni, S.; Koklu, A.; Díaz-Galicia, E.; Moser, M.; Hama, A.; Alqahtani, A. A.; Ahmad, A. N.; Alhamlan, F. S.; Shuaib, M.; Pain, A.; McCulloch, I.; Arold, S. T.; Grünberg, R.; Inal, S. Rapid Single-Molecule Detection of COVID-19 and MERS Antigens via Nanobody-Functionalized Organic Electrochemical Transistors. Nat Biomed Eng 2021, 5 (7), 666–677. https://doi.org/10.1038/s41551-021-00734-9.
33. Jang, H.-J.; Ahn, J.; Kim, M.-G.; Shin, Y.-B.; Jeun, M.; Cho, W.-J.; Lee, K. H. Electrical Signaling of Enzyme-Linked Immunosorbent Assays with an Ion-Sensitive Field-Effect Transistor. Biosensors and Bioelectronics 2015, 64, 318–323. https://doi.org/10.1016/j.bios.2014.09.020.
34. Engvall, E.; Perlmann, P. Enzyme-Linked Immunosorbent Assay (ELISA) Quantitative Assay of Immunoglobulin G. Immunochemistry 1971, 8 (9), 871–874. https://doi.org/10.1016/0019-2791(71)90454-X.
35. Engvall, E. [28] Enzyme Immunoassay ELISA and EMIT. In Methods in Enzymology; Immunochemical Techniques, Part A; Academic Press, 1980; Vol. 70, pp 419–439. https://doi.org/10.1016/S0076-6879(80)70067-8.
36. Ferraris, S.; Cazzola, M.; Peretti, V.; Stella, B.; Spriano, S. Zeta Potential Measurements on Solid Surfaces for in Vitro Biomaterials Testing: Surface Charge, Reactivity Upon Contact With Fluids and Protein Absorption. Frontiers in Bioengineering and Biotechnology 2018, 6, 60. https://doi.org/10.3389/fbioe.2018.00060.
37. Corbett, J. C. W.; McNeil-Watson, F.; Jack, R. O.; Howarth, M. Measuring Surface Zeta Potential Using Phase Analysis Light Scattering in a Simple Dip Cell Arrangement. Colloids and Surfaces A: Physicochemical and Engineering Aspects 2012, 396, 169–176. https://doi.org/10.1016/j.colsurfa.2011.12.065.
38. Karnal, P.; Jha, A.; Wen, H.; Gryska, S.; Barrios, C.; Frechette, J. Contribution of

Surface Energy to PH-Dependent Underwater Adhesion of an Acrylic Pressure-Sensitive Adhesive. Langmuir 2019, 35 (15), 5151–5161. https://doi.org/10.1021/acs.langmuir.9b00120.

39. Hu, Y.; Doudevski, I.; Wood, D.; Moscarello, M.; Husted, C.; Genain, C.; Zasadzinski, J. A.; Israelachvili, J. Synergistic Interactions of Lipids and Myelin Basic Protein. PNAS 2004, 101 (37), 13466–13471. https://doi.org/10.1073/pnas.0405665101.
40. Pawłowski, P. H.; Pawłowski, P. H. Charged Amino Acids May Promote Coronavirus SARS-CoV-2 Fusion with the Host Cell. AIMSBPOA 2021, 8 (1), 111–120. https://doi.org/10.3934/biophy.2021008.
41. Hassanzadeh, K.; Perez Pena, H.; Dragotto, J.; Buccarello, L.; Iorio, F.; Pieraccini, S.; Sancini, G.; Feligioni, M. Considerations around the SARS-CoV-2 Spike Protein with Particular Attention to COVID-19 Brain Infection and Neurological Symptoms. ACS Chem. Neurosci. 2020, 11 (15), 2361–2369. https://doi.org/10.1021/acschemneuro.0c00373.
42. Kun, R.; Szekeres, M.; Dékány, I. Isothermal Titration Calorimetric Studies of the PH Induced Conformational Changes of Bovine Serum Albumin. J Therm Anal Calorim 2009, 96 (3), 1009–1017. https://doi.org/10.1007/s10973-009-0040-5.
43. Tsitsilashvili, E.; Sepashvili, M.; Chikviladze, M.; Shanshiashvili, L.; Mikeladze, D. Myelin Basic Protein Charge Isomers Change Macrophage Polarization. J Inflamm Res 2019, 12, 25–33. https://doi.org/10.2147/JIR.S189570.

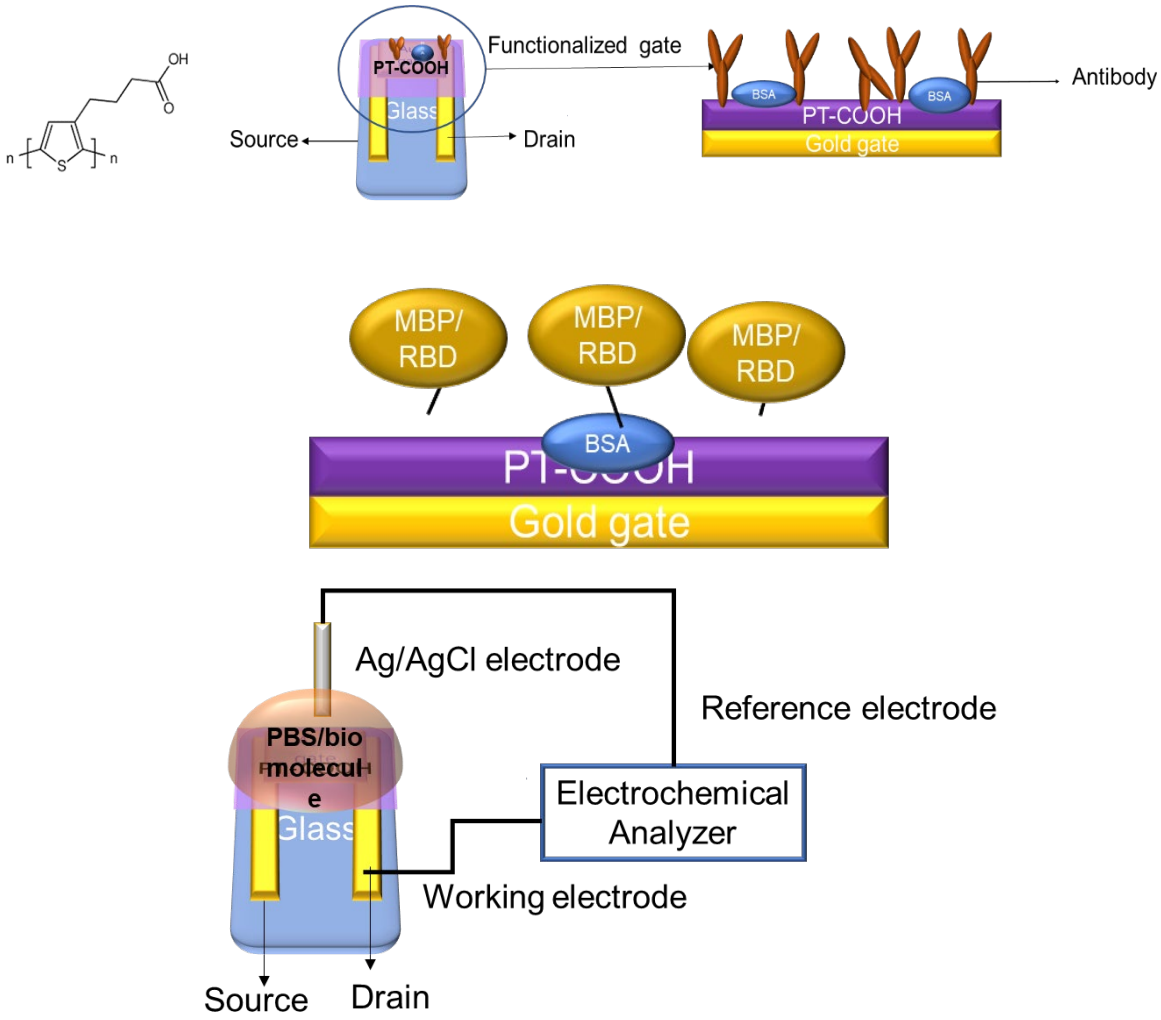

Scheme 1. PT-COOH structure, OECT structure; antibody immobilization method schematic image and protein immobilization method schematic image; Configuration of open circuit measurement.

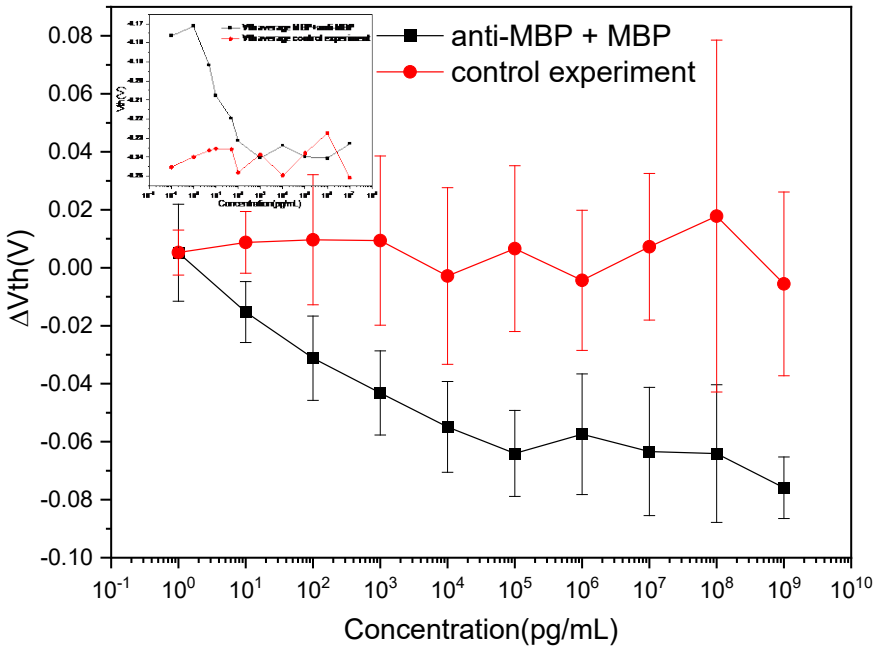

Figure 1. Average threshold voltages were calculated from control and main experiment, and the changes of threshold voltages are indicated in this figure when different concentrations of MBP were added for main experiment and control experiment. All the biomolecules were diluted in 0.05X PBS solution and all the experiments were repeated at least on 4 samples. The inset indicates the average value.

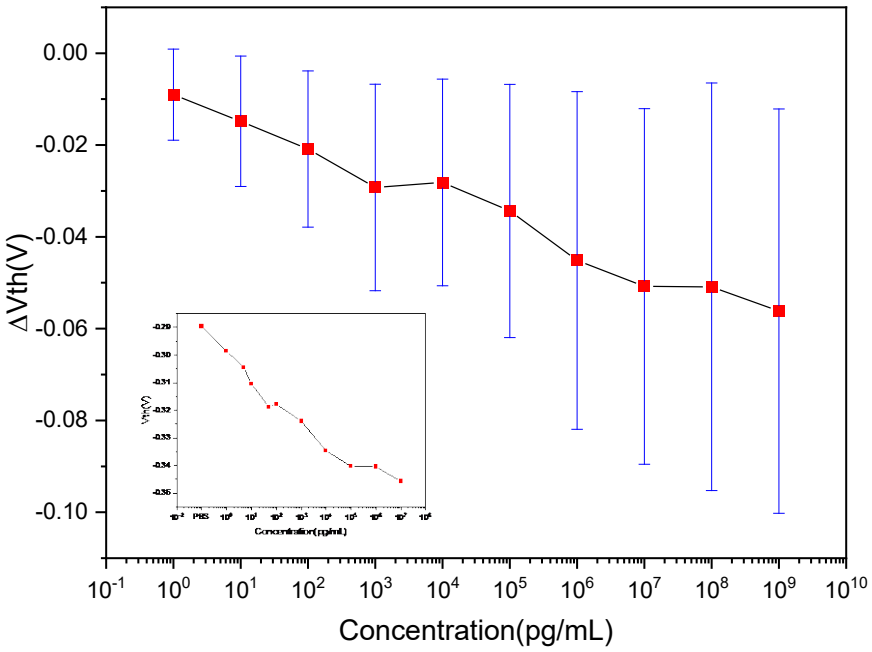

Figure 2. Average threshold voltages were calculated from transfer curves of anti-MBP receptor/MBP analyte, and the changes of threshold voltage are indicated when different concentrations of MBP were added for the main experiment. All the biomolecules were diluted in 1X PBS solution, and all the experiments were repeated at least on 4 samples. The inset indicates the average value.

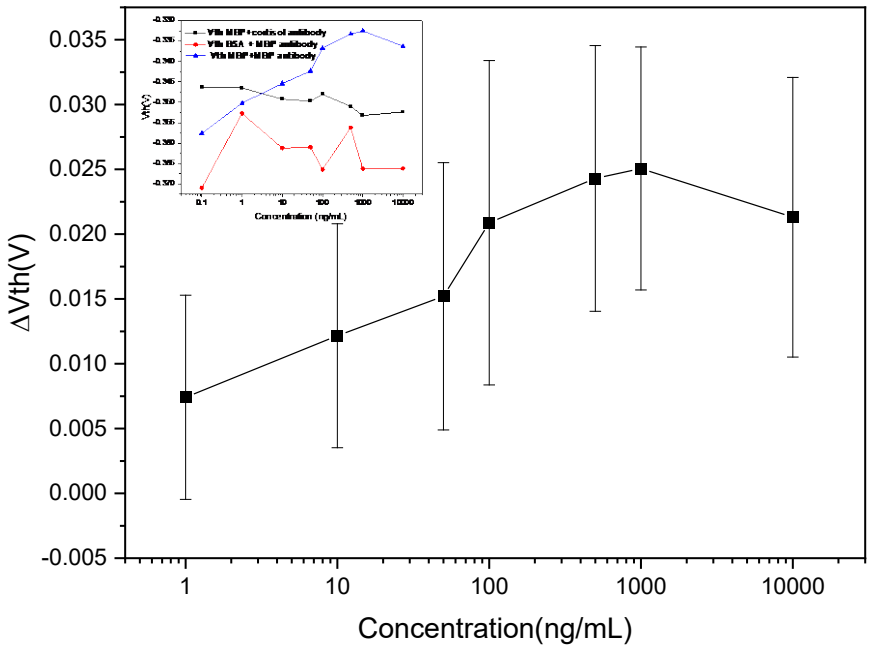

Figure 3. Average threshold voltages were calculated from transfer curves of surface MBP & cortisol antibody analyte control experiment, surface BSA & MBP antibody analyte control experiment and surface MBP & anti-MBP analyte main experiment. The changes of threshold voltage are indicated in this figure when different concentrations of MBP antibody were added for the main experiment. All the experiments were repeated at least on 4 samples. The inset indicates the average value.

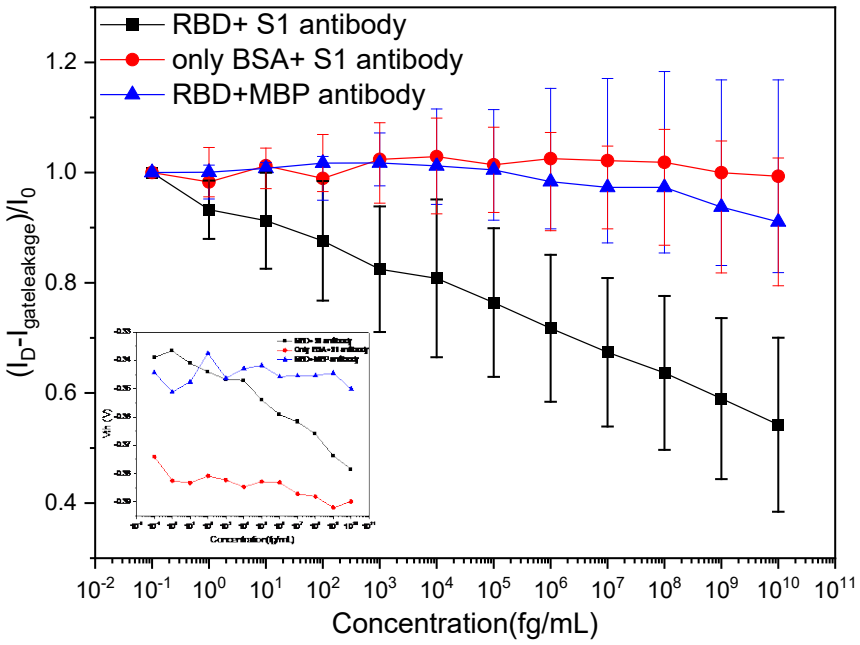

Figure 4. Average threshold voltages were calculated from the transfer curves of different concentration. The blue line is RBD with MBP antibody, the black line is the main experiment which is RBD with S1 protein antibody and the red line is only BSA with S1 protein antibody. Relative current change with different concentration. I_D is the measured drain current, $I_{gate\ leakage}$ is the current caused by gate leakage and I_0 is the drain current when no antibody is added (pure PBS) as analyte. At least three samples were measured at each point. The inset indicates the average threshold voltage value.

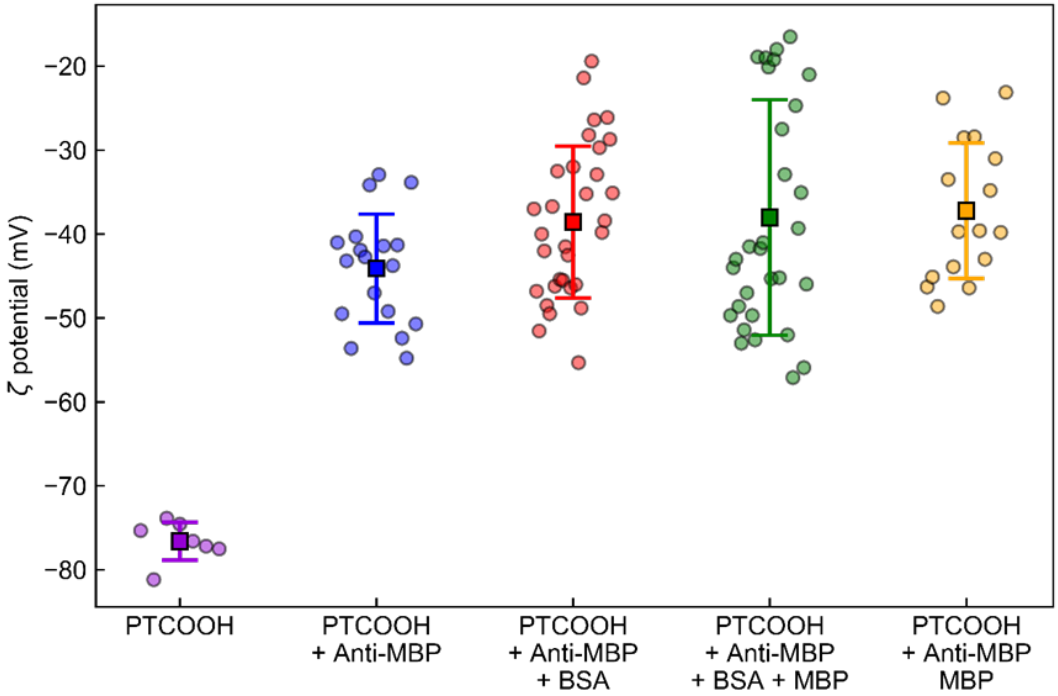

Figure 5. Average surface zeta potential for PTCOOH film, PTCOOH film with MBP antibody immobilization, PTCOOH film with MBP antibody and BSA and PTCOOH film with MBP antibody, BSA and MBP

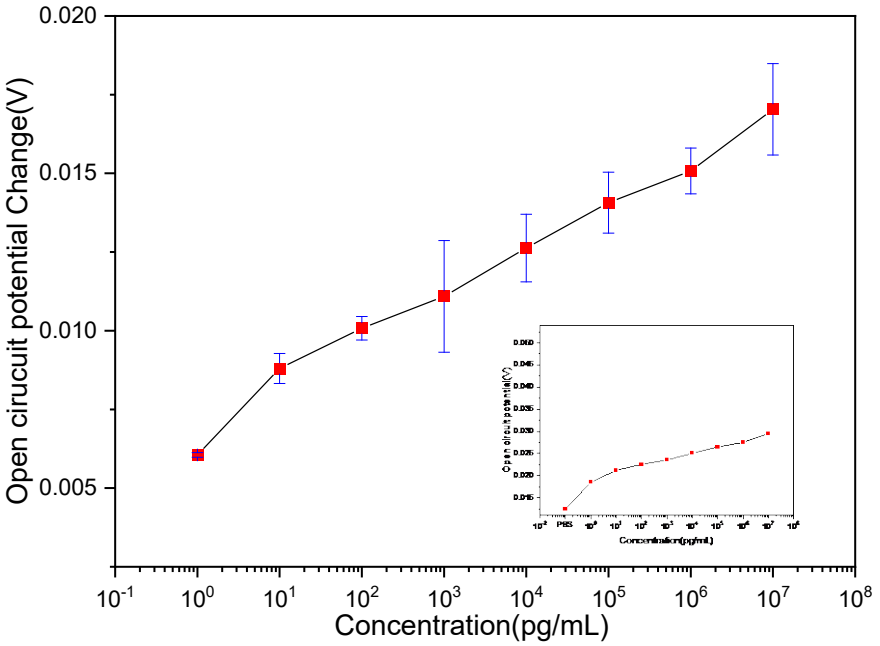

(a)

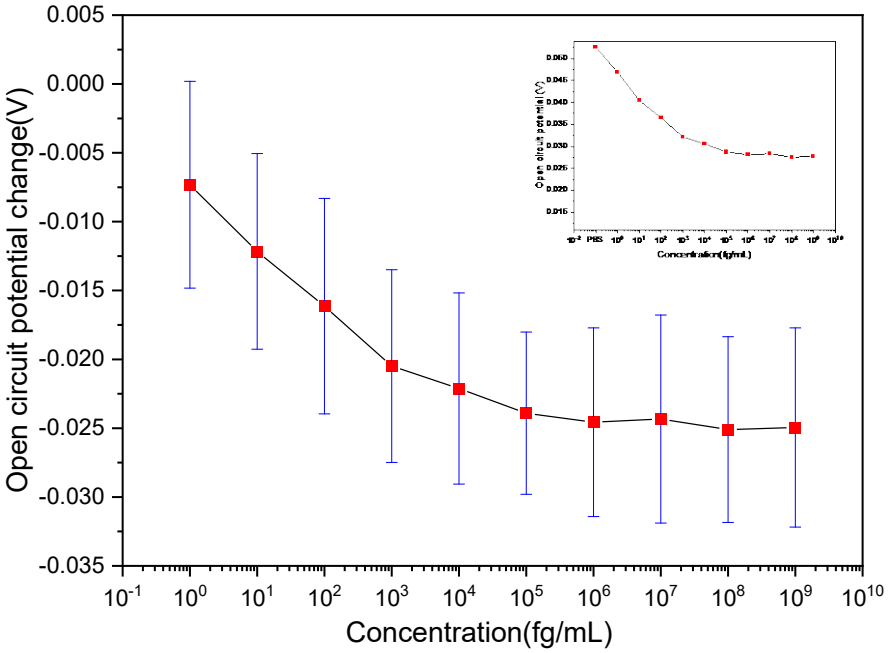

(b)

Figure 6. (a) Average open circuit potential value and open circuit potential change versus different concentration of MBP. (b) Average open circuit potential value and open circuit potential change versus different concentration of S1 antibody. The insets indicate the average value.

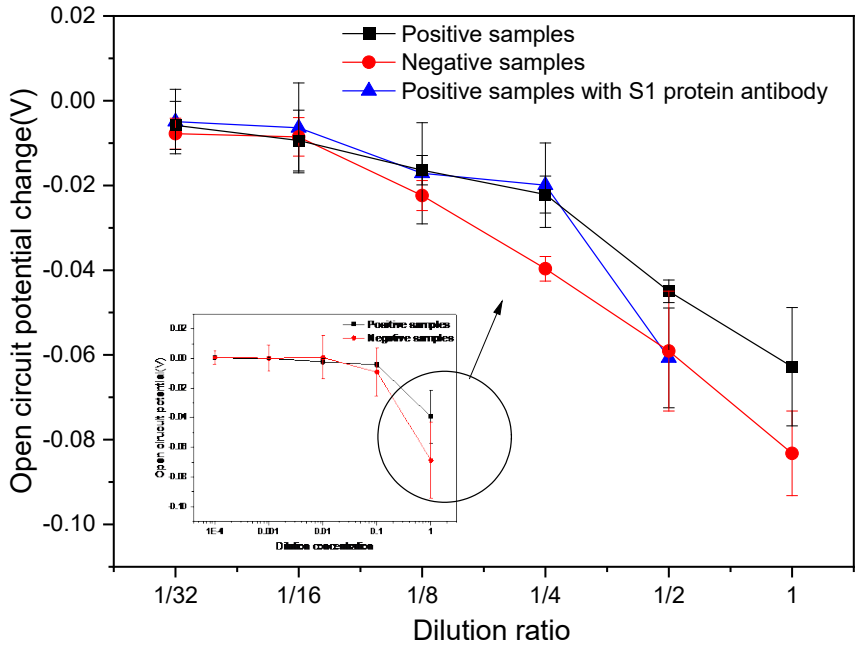

Figure 7. Average open circuit potential change versus different dilution ratio of clinical samples. The main plots show data for a dilution range from about 3% to full concentration. The insets show the lack of change at much lower concentrations. The circles indicate where the main data concentrations would have been on the inset axes.

Table 1. Summary of OECT and OCP Responses.

PT-COOH functionalization[a]	analyte	OECT Vth initial value, subsequent change[b]	Data source	OCP initial value or subsequent change[b]	Data source
none	none	Initial Vth = -0.32 V	Direct measurement	Initial value 40 mV	Section 3.31
BSA(-) only physisorbed[c]	none	Vth = -0.25 (more pos)	Fig 1	--	--
Anti-MBP only[c]	none	--	--	35 mV (slightly more neg)	Section 3.31 and Table S2
Anti-MBP BSA (-) physisorbed	none	Vth – 0.18 (more pos)	Fig 1	12 mV (significantly more neg)	Fig. 6a
Anti-MBP-BSA (-)	MBP(+)	(more neg)	Fig 1	More pos	Fig. 6a
BSA(-) -MBP(+)	none	Vth = -0.36 (more neg)	Fig. 3	52 mV (more pos)	Fig. S2
MBP(+)	Anti-MBP	Slightly more pos	Fig. 3	More neg	Fig. S2
BSA(-) linked no RBD	none	Vth = -0.37 (more neg)	Email 6/24	22 mV (more neg)	Table S2
BSA-RBD(+) control for anti-S1	none	Vth = -0.34 V (more pos vs -0.37 V)	Fig. 4	53 mV (more pos)	Table S2
BSA-RBD(+)	Anti-S1	More neg	Fig. 4	Slightly more neg	Fig. 6b

[a](+) indicates positive net charge on the protein; (-) indicates negative net charge. [b]Directly measured values and/or points designated as “PBS” (zero analyte concentration) on plots. “Pos” and “neg” refer to trends as additional surface functionalization occurred or analyte concentrations were increased. [c]For omitted data, not relevant to those device layers.

For Table of Contents Only